Carrier Phase Multipath Corrections for GPS-based Satellite Attitude Determination

ANGELA K. REICHERT
Jet Propulsion Laboratory, Pasadena, California

PENINA AXELRAD
University of Colorado, Boulder, Colorado

Corresponding Author:
Penina Axelrad
University of Colorado, CB 431
Boulder, CO 80309

Phone : 303-492-6872
Fax : 303-482-2825
Email : Penina.Axelrad@colorado.edu

ABSTRACT : *Multipath errors in GPS carrier phase data dominate the error budget for short baseline applications such as static and kinematic relative positioning and vehicle attitude determination. This paper demonstrates the high degree of spatial repeatability of these errors for a spacecraft environment and describes a correction technique, termed the sky map method, which exploits the spatial correlation to correct measurements and improve the accuracy of GPS-based attitude solutions. Examples of CRISTA-SPAS satellite results are presented.*

Index terms – Global Positioning System, carrier phase multipath, attitude determination

INTRODUCTION

The application of GPS phase measurements to attitude determination of vehicles has been considered since the early 1980's and implemented on a variety of vehicle platforms including marine [1], aircraft [2, 3], land vehicles [4], and spacecraft [5-7]. Cohen [8,9] provides an overview of the principles of GPS phase-based attitude determination and describes several applications. The dominant sources of error for GPS phase-based attitude are baseline flexure on large structures such as aircraft, and multipath for small antenna structures typical of spacecraft installations. The research described here focuses on the correction of multipath for the spacecraft environment.

Carrier phase multipath is the result of interference between signals reflected by surfaces near the receiving antenna and signals arriving via the direct path from the GPS satellite. Both theoretical modeling and experimental evidence shows that multipath can produce phase errors on the order of several mm to several cm in typical spacecraft environments [10] with particularly severe effects on a structure such as the International Space Station [10] or the Space Shuttle [11]. In the last several years significant advances in receiver technology have been made to combat multipath errors in code measurements. While some of these approaches promise to provide improvements in carrier phase errors as well, these have not been widely demonstrated or incorporated into space borne receiver designs.

In the early 1990's Cohen [8] and Cohen and Parkinson [12] identified the spatial repeatability of multipath for a fixed environment and demonstrated a technique for multipath calibration. In particular, they set up a baseline with two antennas and a deliberate reflecting surface on the roof of a building on the Stanford University campus.

By collecting data in several orientations of the baseline over several days they were able to map out a pattern of phase errors introduced. Coefficients of a spherical harmonic model were then fit to the phase errors to produce an approximation that could be used to correct subsequent phase data collected on the array.

We have investigated the application of this type of approach to GPS-based attitude determination of the CRISTA-SPAS spacecraft. CRISTA-SPAS (CRyogenic Infrared Spectrometers and Telescopes for the Atmosphere – Shuttle Pallet Satellite) carried a Trimble TANS-Vector receiver in one of the first space borne experiments in GPS attitude determination [6]. Because the satellite downlinked raw GPS observations, onboard GPS-based attitude solutions, and measurements from an IRU capable of attitude accuracy of 0.05 deg, it serves as an ideal platform for evaluating the accuracy of GPS-based observations and solution techniques [13]. In particular, we have identified large spatially correlated phase residuals in both the phase and signal-to-noise ratio (SNR) data from CRISTA-SPAS that appear to be indicative of a substantial multipath environment [13, 14].

The remainder of the paper begins with a brief overview of the CRISTA-SPAS mission. Next, a method for baseline and line bias calibration using the differential phase data is presented. In the following section, the residual carrier phase data are analyzed for spatial repeatability by comparing residual phase data from different satellites with similar line of sight vectors. Once repeatability has been verified, the spatial sky map method is implemented and attitude solution improvements are presented. Additional results and a more comprehensive explanation of the algorithms can be found in Reichert [15].

CRISTA-SPAS BACKGROUND

The CRISTA-SPAS satellite was successfully launched on November 3, 1994 onboard the STS-66 Space Shuttle Atlantis with a primary mission to observe the middle atmosphere of the Earth. After the CRISTA-SPAS satellite was deployed by the crew of Atlantis, it also recorded GPS data from November 4 – 12, 1994, while orbiting at a distance of a few km from the Shuttle.

A photograph of the satellite being released is shown in Figure 1. The locations and numbers of the zenith-mounted GPS antennas displayed in the photograph are given in the diagram in Figure 2. The antenna labeled as "M" is the master antenna. Three baselines are formed including this antenna, with the baseline number corresponding to the slave antenna number. A representation of the orbit local and body-fixed reference frames is also shown in Figure 2. Throughout the mission, three-axis control of the spacecraft was required in order to point a telescope at an area 62.9 km above the WGS-84 ellipsoid. A star tracker / gyro inertial reference unit (IRU) provided attitude information for closed loop control and an Alcatel GPS receiver provided position information [6].

ALGORITHMS

The GPS phase difference measured between one slave antenna and the master is given by,

$$\Delta\phi = \mathbf{b}\cdot\mathbf{e} - k + \beta + \nu = \oplus^{B}\mathbf{j}^{T}\,\mathbf{e}^{B} - k + \beta + \nu \tag{1}$$

or

$$\Delta\phi = \oplus^{B}\mathbf{j}^{T}\,{}^{B}C^{L}\,\mathbf{e}^{L} - k + \beta + \nu \tag{2}$$

where **b** is the baseline vector, **e** is the line of sight vector, k is the integer ambiguity, β is the line bias, and ν includes all measurement errors due to multipath, thermal noise, tracking error, or receiver clock instability. The superscripts on the vectors describe the coordinate frame in which the elements are specified; in particular, a superscript B refers to the body-fixed frame and L is the orbit local frame. The attitude matrix, ${}^{B}C^{L}$, relates the two frames.

The measurement equation (1) can be used to relate the differential phase observations to baseline components in the body frame if the line of sight vector is known in the body frame. This is the approach taken in a baseline survey. For attitude determination the measurement equation (2) is used to relate the observations to the vehicle attitude, where it is assumed that the baseline is known in the body frame and the line of sight vector is known in the orbit frame.

A. *Batch Estimation for Baseline and Line Bias Calibration*

For CRISTA-SPAS and most other satellite applications, an initial estimate of the baseline components in the body frame ($\mathbf{b}^{B}$) is determined using the mechanical specification of the spacecraft. After mounting the antennas on the actual vehicle or on an electrically similar mockup, an improved baseline solution can be obtained in static ground testing. In a ground self-survey, some assumptions about the attitude of the antenna array are imposed or can be measured using an external attitude reference. Careful attention to the self-survey is important for accurate on-orbit performance.

Even with the best ground survey, it is useful to perform an on-orbit baseline calibration, because of the possibility that the baselines and line bias values will change after launch. In [16], Ward and Axelrad explored possible techniques for refining

baseline estimates using on-orbit data. They compared the results using GPS data alone, and using GPS data together with information from a higher-accuracy attitude reference such as an inertial reference unit (IRU). Their conclusion was that if the vehicle undergoes significant attitude motions, it is possible to separate the baseline and attitude states in a sequential or batch estimator using GPS data alone. However, if the vehicle attitude motion is very limited, as was the case of CRISTA-SPAS, the GPS-only combined attitude and baseline solution is not very reliable.

Thus, for our analysis of CRISTA-SPAS multipath, we rely upon data from the IRU for the on-orbit baseline survey. Specifically, the IRU provides an accurate estimate of the local-to-body rotation matrix, ${}^{B}C^{L}$, that is then used to compute the expected or predicted measurement:

$$\Delta\bar{\phi} = \left[{}^{B}\mathbf{j}^{T} \; {}^{B}\bar{C}^{L} \; \mathbf{e}^{L} \right] - \bar{k} + \bar{\beta} \tag{3}$$

The estimate of the integer ambiguity, $\bar{k}$, can be computed directly if the *a priori* baseline and line bias estimates are within a reasonable fraction of a carrier cycle:

$$\bar{k} = \text{round}\left(\left[{}^{B}\mathbf{j}^{T} \; {}^{B}\bar{C}^{L} \; \mathbf{e}^{L} \right] - \Delta\phi \right) \tag{4}$$

where $\Delta\phi$ is the measured differential phase.

Subtracting equation (3) from equation (1), we get the measurement residual,

$$\delta\phi = \Delta\phi - \Delta\bar{\phi} = \left[{}^{B}\mathbf{b}^{B} \cdot {}^{B}\bar{C}^{L} \; \mathbf{e}^{L} \right] + \delta\beta + v \tag{5}$$

where we have assumed that the integer estimate is correct, and the baseline and line bias errors are large compared to the error in the reference attitude and line of sight vector.

To compute improved solutions for the baselines and line biases, we construct the normal equations as follows:

$$\delta\phi_i = \mathbf{H}\mathbf{x}_i, \quad \text{where } \delta\phi_i \equiv \begin{bmatrix} \delta\phi_i^1 \\ \delta\phi_i^2 \\ \vdots \\ \delta\phi_i^n \end{bmatrix} \quad \mathbf{H} \equiv \begin{bmatrix} e_x^1 & e_y^1 & e_z^1 & 1 \\ e_x^2 & e_y^2 & e_z^2 & 1 \\ \vdots & \vdots & \vdots & \vdots \\ e_x^n & e_y^n & e_z^n & 1 \end{bmatrix} \quad \mathbf{x}_i \equiv \begin{bmatrix} \delta b_{x_i} \\ \delta b_{y_i} \\ \delta b_{z_i} \\ \delta\beta_i \end{bmatrix} \quad \text{for } i = 1,2,3 \tag{6}$$

The subscript i refers to the baseline number and the numbers 1 through n refer to the satellites at each epoch. Note that the baselines and line bias estimates for each baseline are independent of the estimates for the other baselines. Also note that the measurement partial matrix, **H**, is not a function of the baseline, but only of the satellite line of sight vector components expressed in the body frame.

The corrections to the baseline vectors and line biases are computed by solving equation (6) in a least squares sense. The solution may be iterated to insure that the integer values computed in equation (4) do not change. Once the final baselines and line bias estimates, $\hat{\mathbf{b}}$ and $\hat{\beta}$, have been computed using a sufficiently large data set and an accurate attitude reference, the post-fit residuals may be computed. These residuals should be dominated by measurement errors; however, time-varying errors such as baseline variations caused by flexure in the spacecraft body or line bias changes due to temperature variations will also cause residual errors in the signal.

B. Attitude Point Solution Algorithm

If the baselines are known in the body frame, an attitude solution may be found based on GPS observations from a single epoch. This is referred to as an attitude point solution. Various methods for forming attitude point solutions are presented in [8, 9, and 13]. Here we use the method from Ward [13]. By subtracting equation (4) from Equation (2), we

now have an expression for the measurement residual that is a function of the error in the attitude. This may be parameterized in terms of small corrections to angle estimates or quaternions; we use the quaternion implementation by Ward [13]. Figure 3 shows the IRU attitude and the GPS-based attitude point solutions for a 4 hour period. From these graphs one can see both correlated and random errors in the GPS solutions. The following sections will show the improvements that can be obtained by compensating for the spatially correlated errors.

C. Algorithms for Sky Map Construction

Given an estimate of the baselines, line biases, and attitude of the vehicle, a predicted or computed measurement can be formed. The difference between this computed value and the measured value is referred to as the post-fit residual. If the solutions are correct, the post-fit residual should be primarily due to spatially correlated multipath, $\delta\phi_m$, and uncorrelated measurement errors, v_r:

$$\delta\hat{\phi} = \Delta\phi - \Delta\hat{\phi} = v = \delta\phi_m + v_r \tag{7}$$

We have considered two types of post-fit residuals – those based on IRU attitude predictions and those from GPS attitude point solution estimates. In the former case, the attitude estimate is not corrupted by multipath, so we would expect to see more clearly the multipath in the residuals. The latter represents a more realistic situation, in which an external attitude reference is not available. Thus, we hope to see whether multipath correction is still possible using only GPS data.

To construct the sky maps, the residuals for an entire data set are sorted for each baseline independently, as a function of the line of sight vectors in the body-fixed reference frame. Thus, for each residual phase measurement, the corresponding azimuth and elevation of the incoming signal are computed from the three rectangular components of the line of sight vector as follows:

$$az = \text{atan2}\left(e_y^B, e_z^B\right), \qquad el = -\text{asin}\left(e_x^B\right) \tag{8}$$

Note that the x-component of the line of sight vector is down relative to the zenith angle. Several methods are developed here in order to represent the carrier phase errors as a function of the direction of the incoming signal: a spherical harmonic fit, a correction grid, and a two-dimensional polynomial fit. These three methods are described in the sections below.

1) Spherical Harmonic Fit

The first method implemented is the one developed in Cohen and Parkinson [12] and Cohen [8]. Differential phase errors are modeled by a spherical harmonic approximation in the form:

$$\delta\phi_m(el, az) = \sum_{l=1}^{n} J_l P_l[\cos(el)] + \sum_{m=1}^{l} P_{lm}[\cos(el)](C_{lm}\cos(m\,az) + S_{lm}\sin(m\,az)) \tag{9}$$

where P_{lm} are Legendre polynomials and n is the order of the spherical harmonic model. The coefficients of the spherical harmonic model are J_l, C_{lm}, S_{lm} and are determined by rearranging equation (9) into a set of normal equations and solving for the coefficients using a least squares fit to the residual phase errors. For a more complex

reflective surface geometry, the order of the model, n, is increased to account for the typically higher frequency of variation in the multipath that occurs with increased complexity. The number of data points available limits the order of the spherical harmonic fit.

2) Polynomial Fit

As an alternative model to the spherical harmonic fit, a two dimensional polynomial fit is used to represent the phase residuals. Here, the polynomial fit is not defined as a direct function of the azimuth and elevation angles. Making the fit a function of the azimuth and elevation would result in large variations in the zenith direction, where the azimuth lines come very close together, and very small variations on the horizon, where the azimuth lines are much farther apart. Instead, the two dimensional polynomial is modeled as a function of the rectangular coordinates, *x* and *y*, defined as follows:

$$x = (90 - el)\cos az \qquad y = (90 - el)\sin az \tag{10}$$

Using these values, the model for the two dimensional polynomial fit is

$$\delta\phi_m(x,y) = A_0 + \sum_{i=1}^{n}\sum_{j=1}^{n} A_{ij}x^i y^j \tag{11}$$

where n is the order of the polynomial fit. As with the spherical harmonic fit, the order of the model is increased to account for more complex reflector geometry, while being limited by the amount of data available.

3) Correction Grid

A third method is used to model the residual phase as a function of the line of sight vector. This method uses the x, y variables in equation (10) to define a rectangular

region. The region is then divided into a grid of bins of a certain size, defined as δx by δy. Then, each residual phase measurement is placed into a bin corresponding to the x and y value for that signal. A phase correction value is assigned to each bin by taking the mean of all of the values within a bin. If too few data points are available because spatial coverage is limited, the size of the bins may be increased to supply a better representation of the data. The correction value for the individual data points is applied either by interpolation or as a table lookup.

RESULTS OF BASELINE AND LINE BIAS CALIBRATION

Before the residual differential phase values are computed from the CRISTA-SPAS differential phase data, the baselines and line biases are calibrated using the batch filter described previously with the entire 32 hours of data. The tracks for the line of sight vectors for all 32 hours of data are shown on the polar plot in Figure 4. The offset of the pattern from the center of the plot is due to the nominal off-nadir orientation of the vehicle body to point the telescope in the preferred direction. Table 1 contains the initial estimates for the baselines in the mechanical body-fixed frame, based on the CRISTA-SPAS mechanical drawings [13]. The batch filter is applied using the entire set of measured minus computed differential phase data and the local to body rotation matrix as determined from the IRU reference quaternions. Measurement data in which the phase residuals are greater than a quarter of a cycle are excluded from the processing in order to avoid including anomalous measurements in the calibration. The calibrated baselines and line biases as expressed in the IRU body-fixed frame, are also shown in Table 1.

Note that the estimates of the baseline components differ from the nominal values by as much as 1 cm. For a baseline length of approximately 1 m, this corresponds to an attitude error of 10 mrad, or approximately 0.57 deg. The discrepancy between the baseline values in the two frames could be due to either a shift in the electrical phase center of the antenna after the satellite was deployed or a slight misalignment between the mechanical and IRU body-fixed frames. After baseline and line bias calibration, the differential phase residuals will contain errors due only to temporal variations in the baselines and line biases, measurement noise and multipath.

Table 1: CRISTA-SPAS baselines from mechanical drawings and based on flight data.

	BASELINE	x(m)	y(m)	z(m)	line bias (cycles)
Mechanical	1	-0.0325	0.7498	0.6620	
Drawings	2	0.0060	0.3265	1.2350	
	3	-0.0325	-0.4233	0.6620	
On Orbit	1	-0.0198	0.7525	0.6635	0.1399
Calibration	2	0.0175	0.3334	1.2423	0.0114
	3	-0.0237	-0.4170	0.6680	0.2584

SPATIAL REPEATABILITY OF THE CRISTA-SPAS PHASE AND SNR MEASUREMENTS

Before the CRISTA-SPAS data were processed using the sky map method, the spatial repeatability of the data was tested. This was done by identifying GPS satellite tracks that follow similar paths. In this testing, four such paths are identified. Because each of these paths traverse the same region of the sky, they should view similar multipath trends in both the SNR and the carrier phase, if indeed multipath is spatially correlated. The azimuth and zenith angles of the four tracks chosen for evaluation are shown in a polar plot in Figure 5. The SNR and IRU-based residual differential phase for these satellite passes are shown in Figure 6 and 7, respectively.

Since the residual differential phase follows the same trends for the satellite passes at different times, it can be inferred that the data are highly spatially correlated. Thus, one would expect a mitigation method utilizing this fact to be effective in reducing multipath in the received signal. In addition, results computed using a specific period in time should be valid for the same section of the sky at some later point in time.

RESIDUAL PHASE MAP MULTIPATH CORRECTION

Using the baseline and line bias values shown in Table 1, and the IRU reference quaternions, the ideal GPS differential phase residuals are computed. Then, the correction maps are computed using all 32 hours of the CRISTA-SPAS residual phase data.

Correction maps for baseline 1, computed using a one 1 deg by 1 deg grid fit, a twelfth order spherical harmonic fit, and a sixth order two dimensional polynomial fit are shown in Figures 8-10. Illustrations of the sky maps for the other baselines can be found in Axelrad and Reichert [17]. Note that these maps are plotted as a function of the rectangular values, x and y, as shown in equation (10). The grid fit is termed a 1 deg by 1 deg fit because the bin size for the fit corresponds to a δx and δy size each of 1 deg. Additionally, both a 2 deg and a 4 deg bin size case and an eighth order spherical harmonic fit were computed.

In all three of the maps for baseline 1 shown above, there exists a region of severe multipath in the lower right portion of the map. The errors range from approximately -4 to +4 cm and exist in an area from approximately 0 to 45 deg in elevation. Similar, but not quite as large, phase errors are also seen in the other two baselines in all of the other maps for the same region of the sky.

Table 2 shows the RMS of the IRU-based residual phase improvements using each of the three methods for all three baselines. Note that the raw residuals are smallest for baseline 3 with a residual RMS of 7.8 mm and largest for baseline 1 with an RMS of 9.6 mm. The 1 deg by 1 deg correction grid is shown to provide the best fit to the phase residuals by reducing the residuals to the range of 4.2 to 4.6 mm. The large reduction in the residual phase indicates that in fact, 40 to 50 percent of the differential phase error is

spatially correlated. The remaining 4 to 5 mm of error is likely due to high frequency phase noise and perhaps a smaller low frequency error is due to baseline and line bias variation.

Table 2 also shows the residual statistics for a 1 deg by 1 deg grid based on point solution residuals rather than IRU attitude solutions. In this case the GPS data have been used to construct a point solution and then the post-fit residuals are assembled into the correction grid. The raw residuals from the point solution are smaller, as expected, because the point solution has absorbed some of the measurement error. However, the reduction in the residual after application of the phase map, shows that even the point solution residuals are highly spatially correlated. Thus, one would expect a sky map correction based only on GPS solutions should provide improvements in the attitude solutions, albeit not as significant as a correction based on an external attitude reference.

The results for the sky maps for the eighth and twelfth order spherical harmonic fits to the residual phase data are also presented in Table 2. The twelfth order spherical harmonic phase map is shown Figure 9. While this figure shows the same general trend as the grid map, it cannot capture the irregularities in the residuals found in the grid map. Spherical harmonics assume a level of symmetry and smoothness for low order models that do not appear to be valid for the CRISTA-SPAS reflector configuration. Furthermore, in a typical spacecraft environment, reflectors are likely to be small, producing spatially discontinuous multipath contributions. A spherical harmonic model would perhaps be more appropriate for ground applications where it is more likely that large surfaces dominate the multipath environment.

The sky map for the polynomial fit is shown in Figure 10. The residual and attitude improvements when using the polynomial fit are shown in the tables below. As seen in the figure, the polynomial fit is capable of representing steep residual gradients near the edges of the map, where the edges correspond to lower elevation angles. However, false corrections are introduced for high elevation angle satellites, resulting in an overall point solution accuracy similar to the spherical harmonic models.

Table 2: Summary of phase residual statistics for sky map correction algorithms.

	Algorithm	RMS Residuals in mm (% Reduction compared to raw)		
		baseline 1	baseline 2	baseline 3
RAW	IRU-based	9.6	8.7	7.8
	GPS-only	7.8	7.2	6.8
GRID MAP	1 x 1 (IRU-based)	4.7 (51%)	4.2 (52%)	4.6 (41%)
	1 x 1 (GPS-only)	3.3 (58%)	3.5 (52%)	3.6 (47%)
	2 x 2	5.0 (48%)	4.4 (49%)	4.8 (38%)
	4 x 4	5.6 (42%)	4.9 (44%)	5.2 (33%)
SPHERICAL HARMONIC	8^{th} order	6.9 (28%)	6.5 (26%)	6.3 (20%)
	12^{th} order	6.3 (35%)	6.0 (31%)	5.9 (25%)
POLYNOMIAL	6^{th} order	6.9 (28%)	5.9 (32%)	6.3 (20%)

ATTITUDE IMPROVEMENT USING THE CORRECTED PHASE RESIDUALS

The sky map corrections are now applied to the GPS measurements and new attitude point solutions are formed. The statistics of the resulting attitude improvements for all of the phase maps are shown in Table 3. The largest attitude improvements are produced using the phase corrections from the 1 deg by 1 deg grid map constructed from IRU-based residuals. After applying the grid map to the entire set of phase data, the RMS of

the attitude error reduces from 0.25 deg to 0.1 deg in yaw, 0.14 deg to 0.07 deg in roll, and 0.24 deg to 0.18 deg in pitch. Results using the GPS-based residuals are not quite as good, showing final accuracy of 0.16 deg in yaw, 0.1 deg in roll, and 0.21 deg in pitch. The attitude solutions using both 1 deg by 1 deg grid map corrections are shown as a function of time in Figures 11 and 12, respectively.

In addition to the grid map method, results for the spherical harmonic fit and polynomial fit are shown in Table 3 for each of the three baselines. While the sixth order polynomial fit and the eight and twelfth order spherical harmonic fits produced noticeable improvements in the attitude solution, the improvement in attitude error is not as large as with the grid map correction.

Table 3: Summary of attitude point solution statistics for the sky map correction algorithms.

Algorithm		Point Solution RMS Error in deg (% reduction compared to uncorrected.)		
		yaw	roll	pitch
UNCORRECTED	POINT SOLUTION	0.250	0.136	0.239
GRID MAP	1 x 1 (IRU-based)	0.102 (59%)	0.074 (45%)	0.176 (26%)
	1 x 1 (GPS-only)	0.155 (38%)	0.100 (26%)	0.212 (11%)
	2 x 2	0.107 (57%)	0.083 (39%)	0.189 (21%)
	4 x 4	0.125 (50%)	0.097 (28%)	0.200 (16%)
SPHERICAL HARMONIC	8^{th} order	0.172 (31%)	0.120 (12%)	0.211 (11%)
	12^{th} order	0.152 (40%)	0.108 (20%)	0.207 (13%)
POLYNOMIAL	6^{th} order	0.172 (31%)	0.116 (14%)	0.216 (9%)

CONCLUSIONS AND FUTURE WORK

The methods for carrier phase multipath correction presented in this paper were successful in reducing the multipath for data from the CRISTA-SPAS spacecraft. In particular, the grid map method reduced the phase residuals by over 40% for baseline 3

and over 50% for baselines 1 and 2, resulting in an attitude improvement of 59% in yaw, 45% in roll, and 26% in pitch. Moreover, these results indicate that the majority of the error in the signal is spatially correlated and can be reduced using spatial techniques. In a more typical situation where an accurate attitude reference is not available, there is still a significant improvement in the attitude accuracy, but it is less than 40% in each axis. In this situation there is more error in the map due to coupling of the multipath errors into the attitude solutions. For a large data set from a vehicle with larger attitude motions, there should be better separation of multipath from the attitude error.

ACKNOWLEDGEMENT

This research was completed while Dr. Reichert was a research assistant at the University of Colorado. It was supported under grants from the Draper Laboratory.

REFERENCES

1. Lu, G., and M. E. Cannon, *Attitude Determination Using A Multi-Antenna GPS System for Hydrographic Applications*, Marine Geodesy, Vol. 17, 1994, pp. 237-250.

2. Cannon, M.E. and H. Sun, *Assessment of a Non-Dedicated GPS Receiver System for Precise Airborne Attitude Determination, Photogrammetry and Remote Sensing*, Journal of the ISPRS, Vol. 51, pp. 99-108, 1996.

3. Schade, H., M.E. Cannon and G. Lachapelle, *An Accuracy Analysis of Airborne Kinematic Attitude Determination with the NAVSTAR/Global Positioning System*, SPN Journal, Vol. 3, No. 2, pp. 90-95.

4. Harvey, R. and M.E. Cannon, *Operational Results of a Closely Coupled Integrated Vehicle Heading System*, Proceedings of ION GPS-97, Kansas City, September 19-21, 1997, pp. 279-288.

5. Lightsey, E.G., *Development and Flight Demonstration of a GPS Receiver for Space*, Ph.D. Dissertation, Stanford University, February 1997.

6. Brock, J. K., R. Fuller, B. Kemper, D. Mleczko, J. Rodden, A. Tadros, *GPS Attitude Determination and Navigation Flight Experiment*, Proceedings of ION GPS-95, Palm Springs, CA, September 1995, pp. 545-554.

7. Carpenter, J. R., and R. M. Hain, *Precise Evaluation of Orbital GPS Attitude Determination on the STS-77 GPS Attitude and Navigation Experiment (GANE)*, Proceedings of ION National Technical Meeting, January 1997.

8. Cohen, C. E., *Attitude Determination Using GPS,* Ph.D. Dissertation, Stanford University, December, 1992.

9. Cohen, C. E., *Attitude Determination*, in Global Positioning System: Theory and Applications, Vol. 2, B. W. Parkinson et al., eds., AIAA, 1995.

10. Gomez, S. F., R. J. Panneton, P. E. Saunders, S. U. Hwu, B. P. Lu, *GPS Multipath Modeling and Verification Using Geometrical Theory of Diffraction*, Proceedings of ION GPS-95, Palm Springs, CA, September, 1995, pp. 195-204.

11. Gomez, S. F. and S. U. Hwu, *Comparison of Space Shuttle GPS Flight Data to Geometric Theory of Diffraction Predictions*, Proceedings of ION GPS-97, Kansas City, September 19-21, 1997, pp. 605-614.

12. Cohen, C. E. and B. W. Parkinson, *Mitigating Multipath in GPS-Based Attitude Determination*, Advances in the Astronautical Sciences, AAS Guidance and Control Conference, Keystone, CO, Vol. 74, Univelt, San Diego, 1991.

13. Ward, L. M., *Spacecraft Attitude Estimation Using GPS: Methodology and Results*, Ph.D. Dissertation, Department of Aerospace Engineering Sciences, University of Colorado, July 1996.

14. Comp, C. J., *GPS Carrier Phase Multipath Characterization and Mitigation Technique Using the Signal-to-Noise Ratio*, Ph.D. Dissertation, University of Colorado, July 1996.

15. Reichert, A. K., *Correction Algorithms for GPS Carrier Phase Multipath Utilizing the Signal-to-Noise Ratio and Spatial Correlation,* Ph.D Dissertation, Department of Aerospace Engineering Sciences, University of Colorado, December 1999.

16. Ward, L.M. and P. Axelrad, *A Combined Filter for GPS-Based Attitude and Baseline Estimation*, NAVIGATION, Journal of the Institute of Navigation, Vol. 44, No. 2, 1997, pp. 195-213.

17. Axelrad, P. and A. Reichert, *Algorithms for Calibration of Multipath Errors Using Micro-Mechanical Gyros*, Colorado Center for Astrodynamics Final Report for Draper Lab IR&D Project No. 802, July 1997.

Figure 1. Photograph of CRISTA-SPAS (Courtesy of J. Rodden, Loral Space Systems)

Figure 2. CRISTA-SPAS body-fixed and local frames. The locations of the Master (M) and three slave antennas (1-3) are shown. The unit vectors in the body-fixed and local frames are denoted by superscripts, B and L, respectively.

Figure 3: Uncorrected attitude solutions. The IRU reference attitude is represented by the dark line while the attitude point solution, uncorrected for multipath, is shown as the lighter line. The yaw, roll, and pitch angles are shown in the top, middle, and bottom figures, respectively.

Figure 4: Satellite data points for the 32 hours of CRISTA-SPAS data. The data points are shown as a function of azimuth and zenith angle in the satellite local frame.

Figure 5: Four satellite passes following similar tracks, displayed in the CRISTA-SPAS body-fixed reference frame.

Figure 6: SNR for the slave 3 antenna for the four satellite passes. The lines represent four satellite passes occurring at the same spatial location but at different times.

Figure 7: Residual differential phase for baseline one for the four passes. The lines represent four satellite passes occurring at the same spatial location but at different times.

Figure 8: One degree grid fit for baseline 1. The contour map displays residual differential phase errors as a function of the rectangular x-y coordinate location.

Figure 9: Twelfth order spherical harmonic fit for baseline 1. The contour map displays residual differential phase errors as a function of the rectangular *x-y* coordinate location.

Figure 10: Sixth order 2-D polynomial fit for baseline 1. The contour map displays residual differential phase errors as a function of the rectangular *x-y* coordinate location.

Figure 11: Attitude solution after phase correction using the IRU-based 1 degree grid map. The IRU reference attitude is represented by the dark line while the attitude point solution, corrected for multipath using the 1 degree grid map, is shown as the lighter line. The yaw, roll, and pitch angles are shown in the top, middle, and bottom figures, respectively.

Figure 12: Attitude solution after phase correction using the GPS-only 1 degree grid map. The IRU reference attitude is represented by the dark line while the attitude point solution, corrected for multipath using the 1 degree grid map, is shown as the lighter line. The yaw, roll, and pitch angles are shown in the top, middle, and bottom figures, respectively.

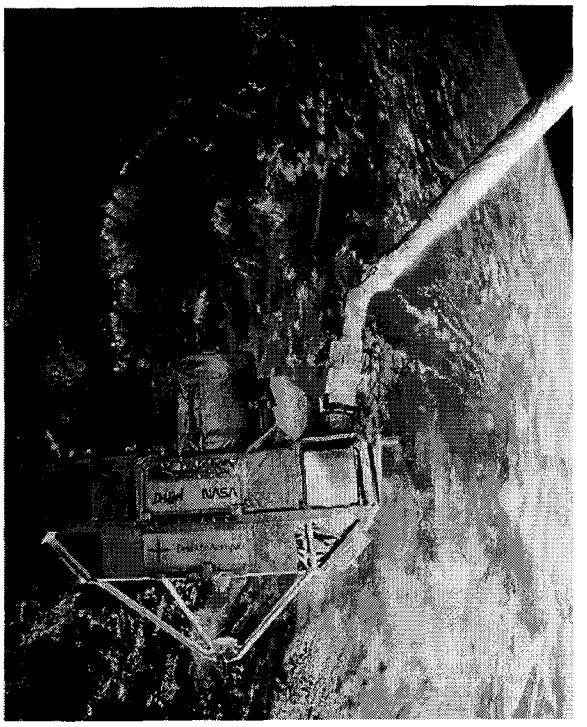

Figure 1

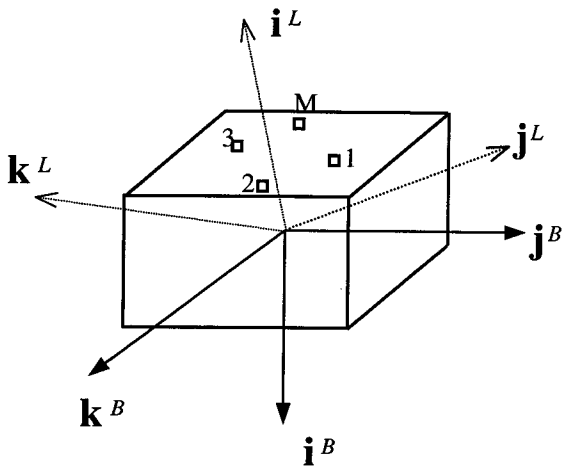

Figure 2

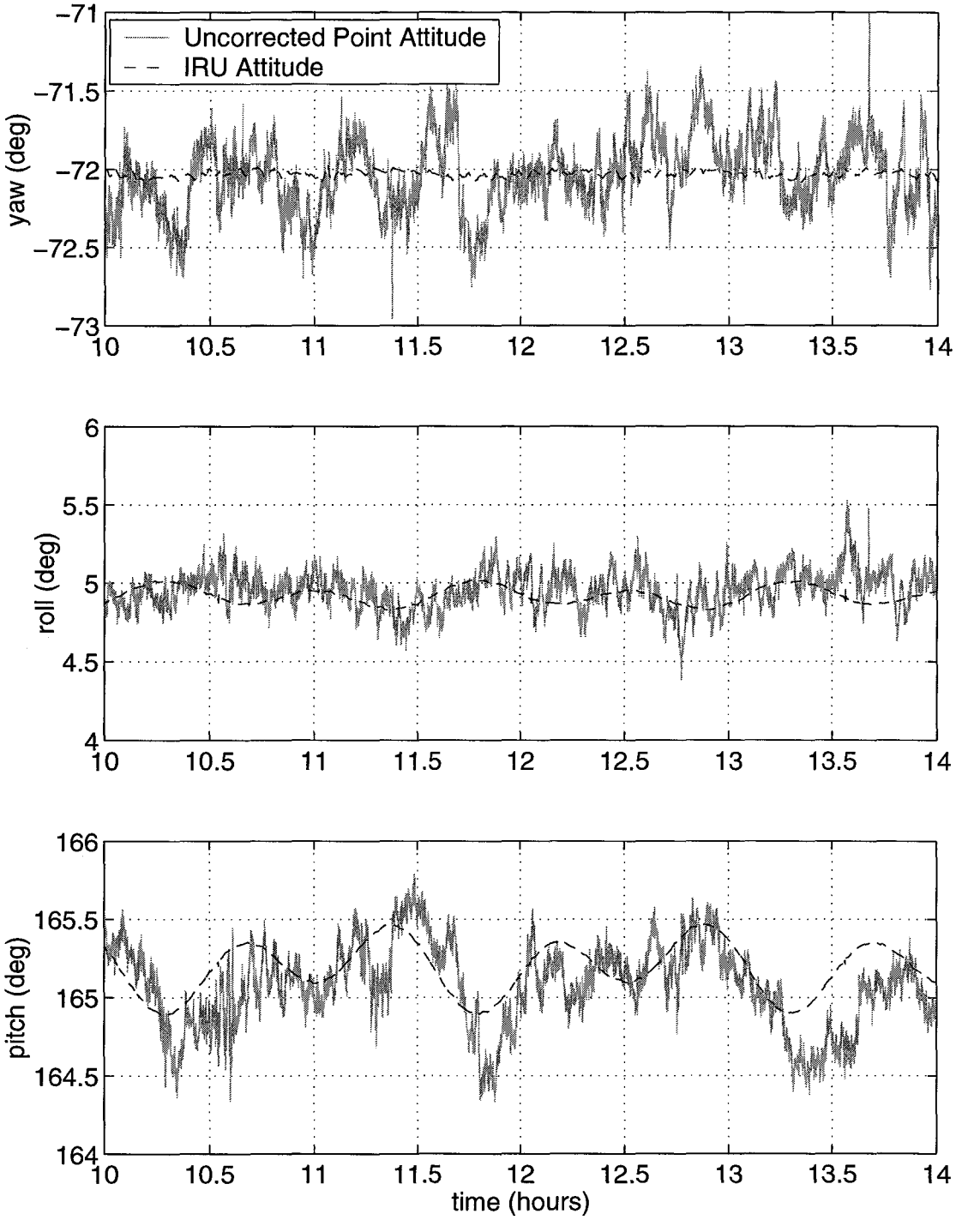
Uncorrected Point Attitude
IRU Attitude
yaw (deg)
roll (deg)
pitch (deg)
time (hours)
−71
−71.5
−72
−72.5
−73
6
5.5
5
4.5
4
166
165.5
165
164.5
164
10
10.5
11
11.5
12
12.5
13
13.5
14

Figure 3

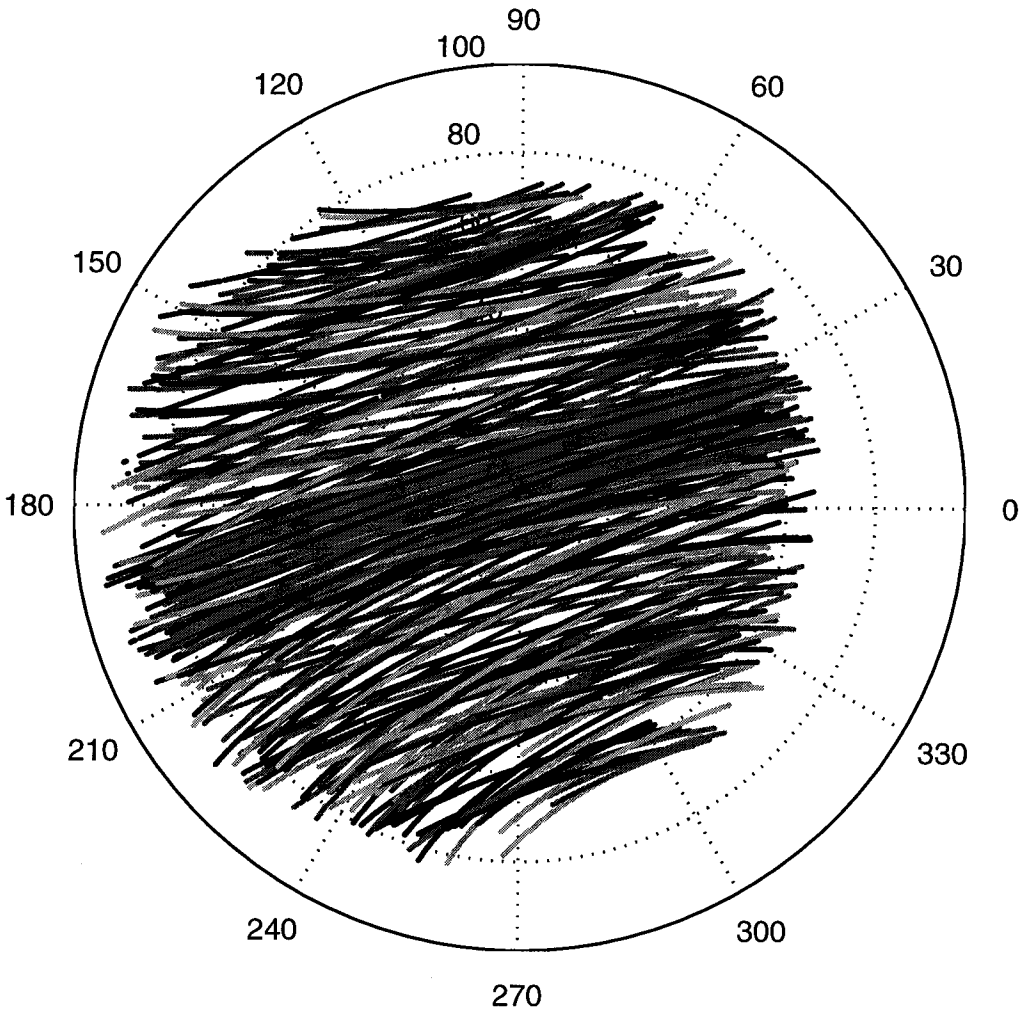

Figure 4

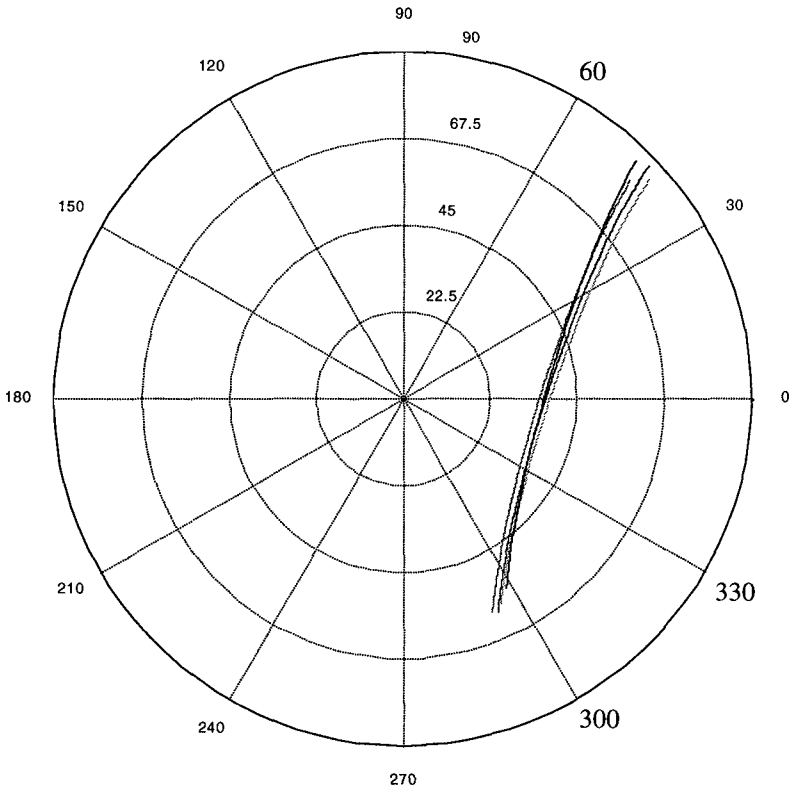

Figure 5

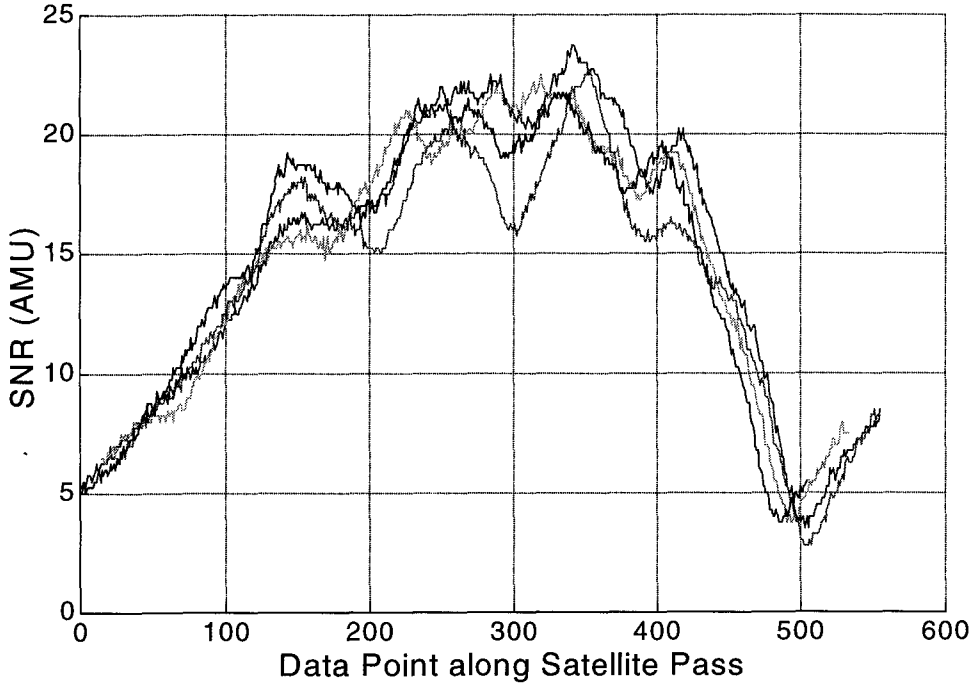
25
20
15
10
5
0
SNR (AMU)
0
100
200
300
400
500
600
Data Point along Satellite Pass

Figure 6

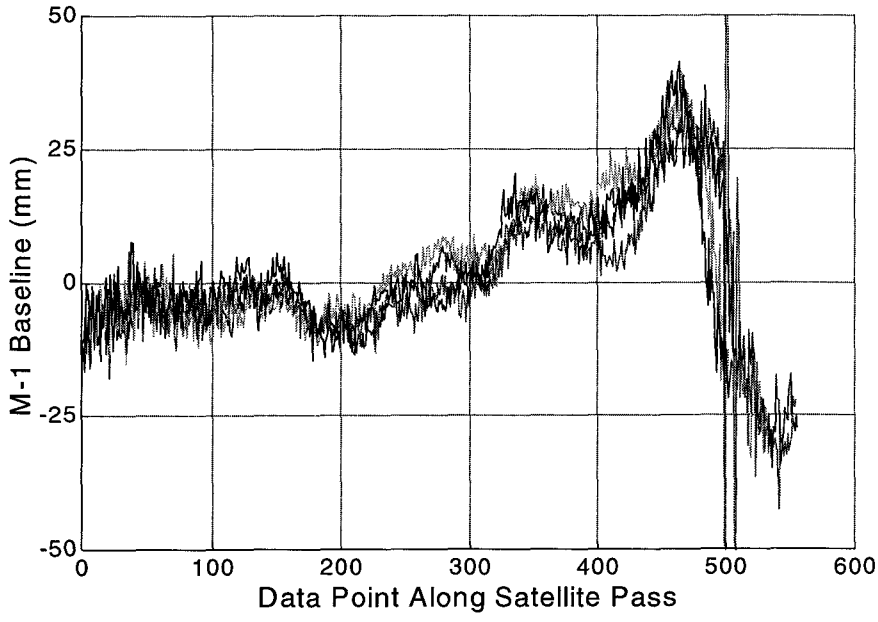
50
25
0
-25
-50
M-1 Baseline (mm)
0
100
200
300
400
500
600
Data Point Along Satellite Pass

Figure 7

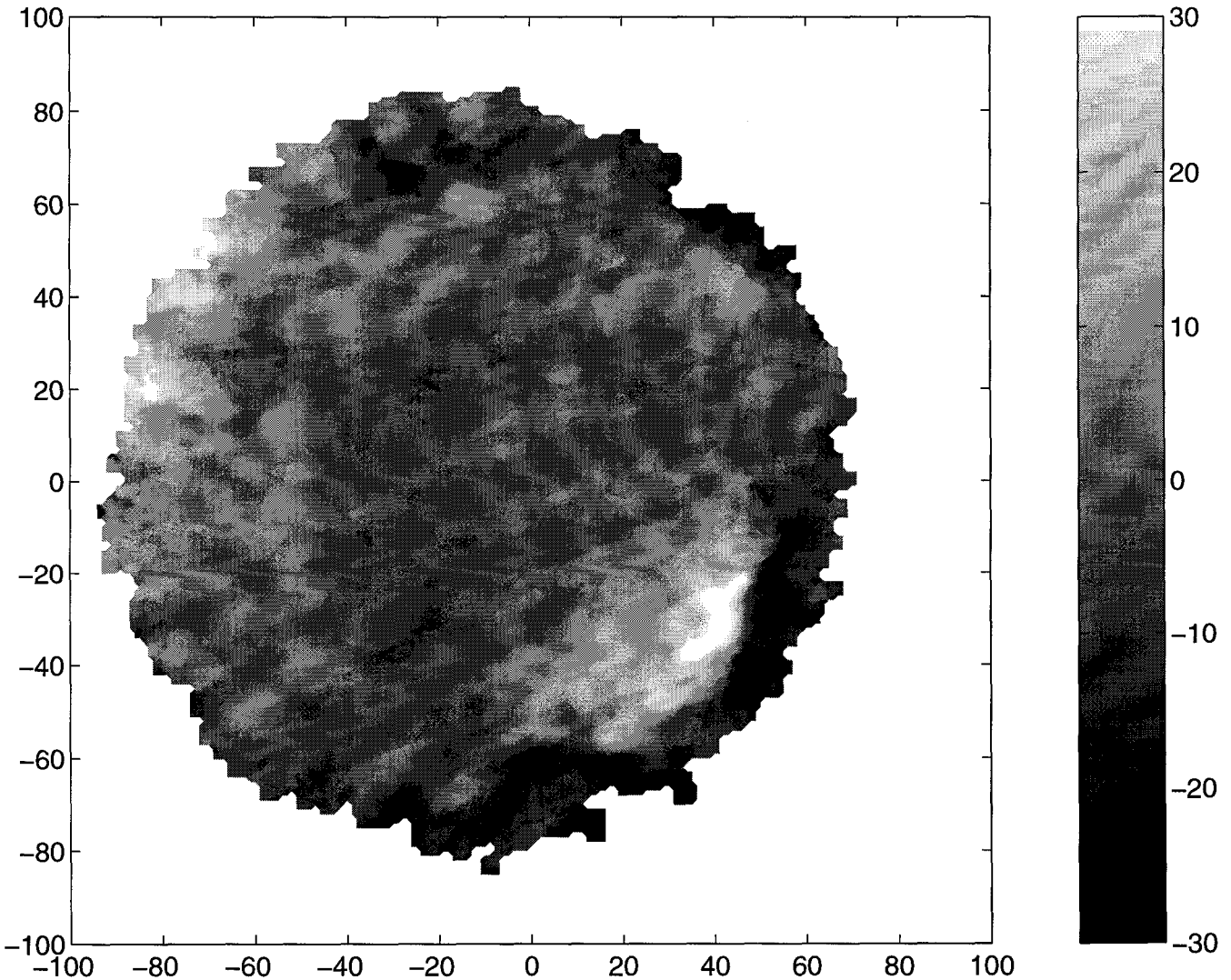
100
80
60
40
20
0
−20
−40
−60
−80
−100
−100
−80
−60
−40
−20
0
20
40
60
80
100
30
20
10
0
−10
−20
−30

Figure 8

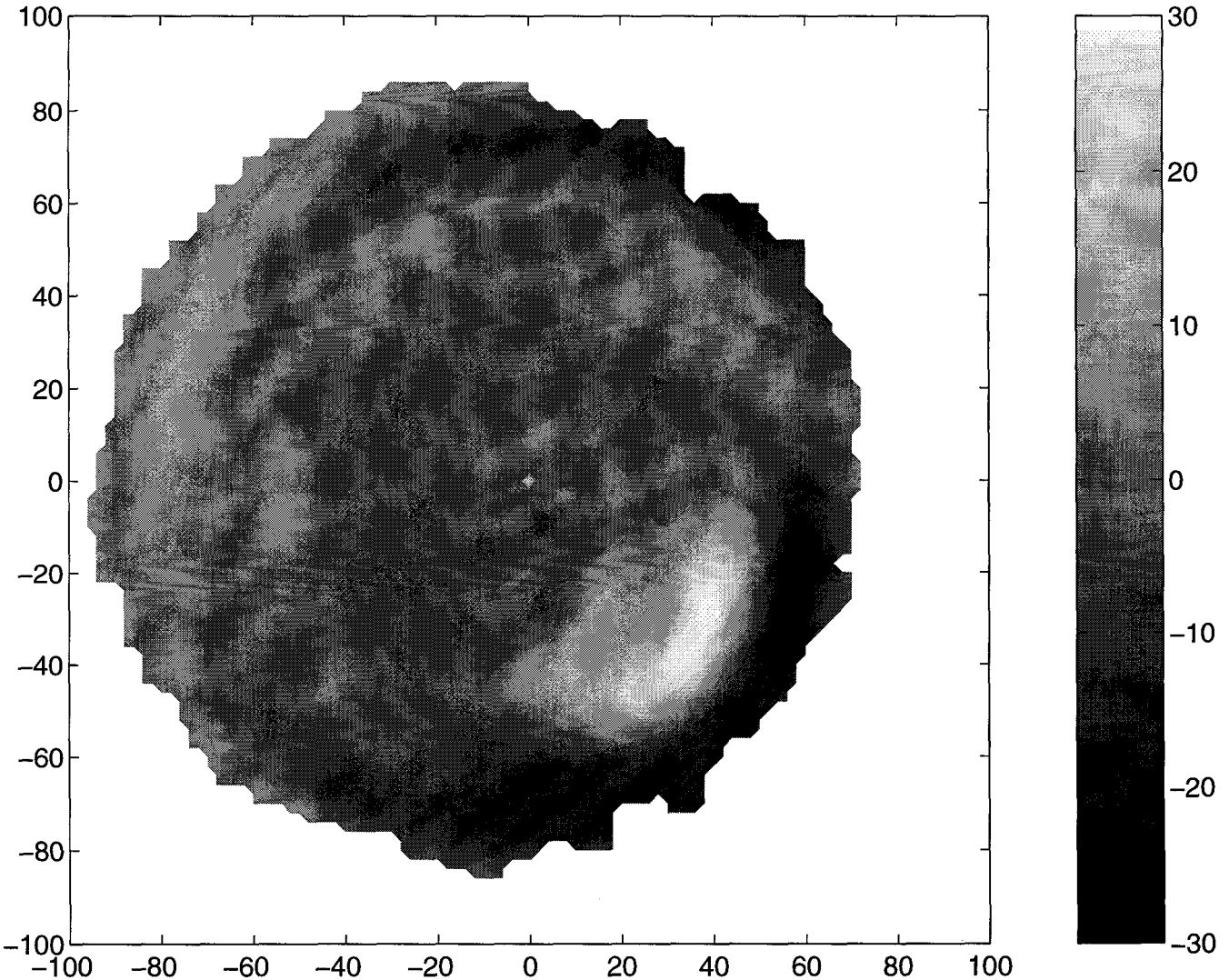
100
80
60
40
20
0
−20
−40
−60
−80
−100
−100
−80
−60
−40
−20
0
20
40
60
80
100
30
20
10
0
−10
−20
−30

Figure 9

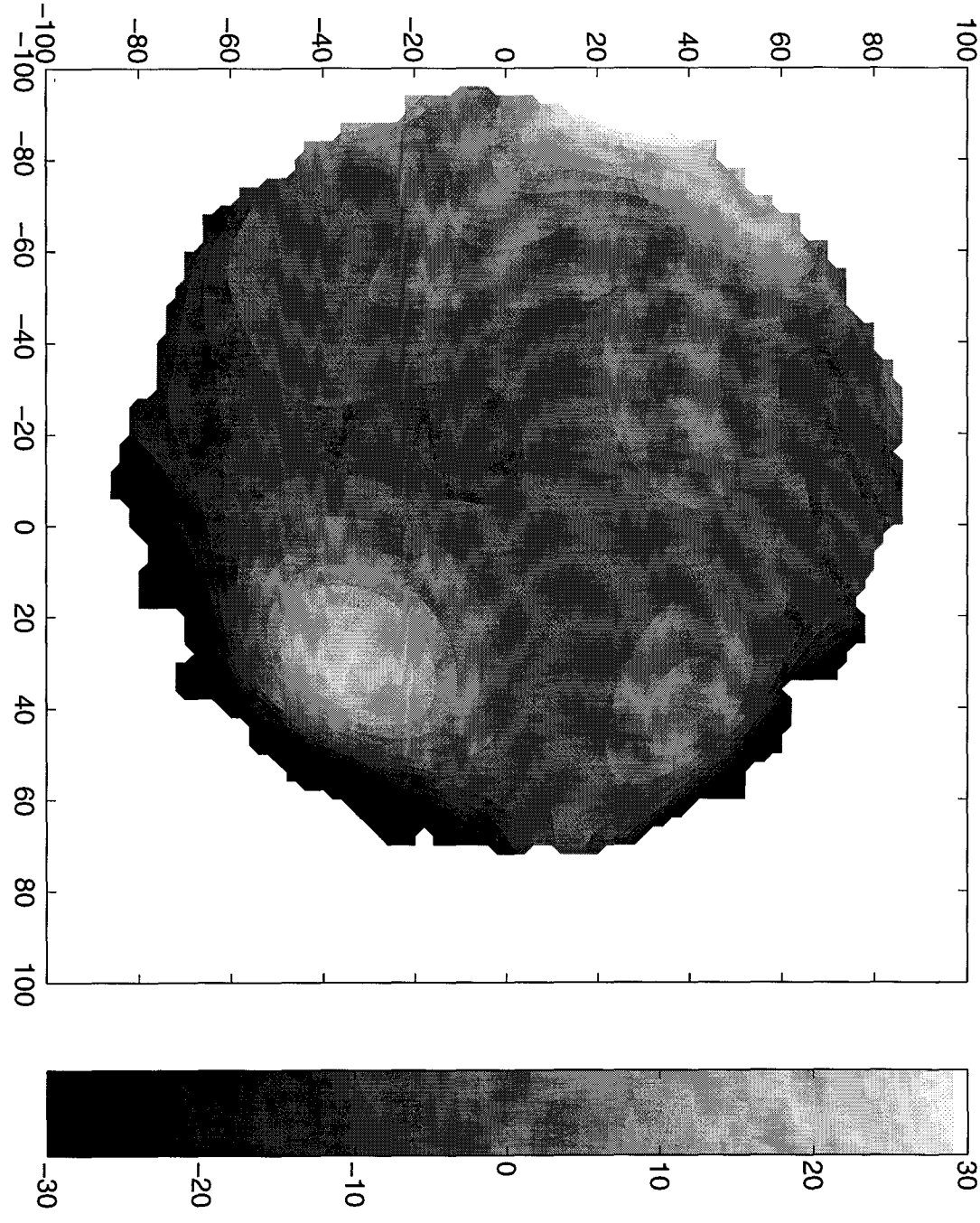
100
80
60
40
20
0
-20
-40
-60
-80
-100
-100
-80
-60
-40
-20
0
20
40
60
80
100
30
20
10
0
-10
-20
-30

Figure 10

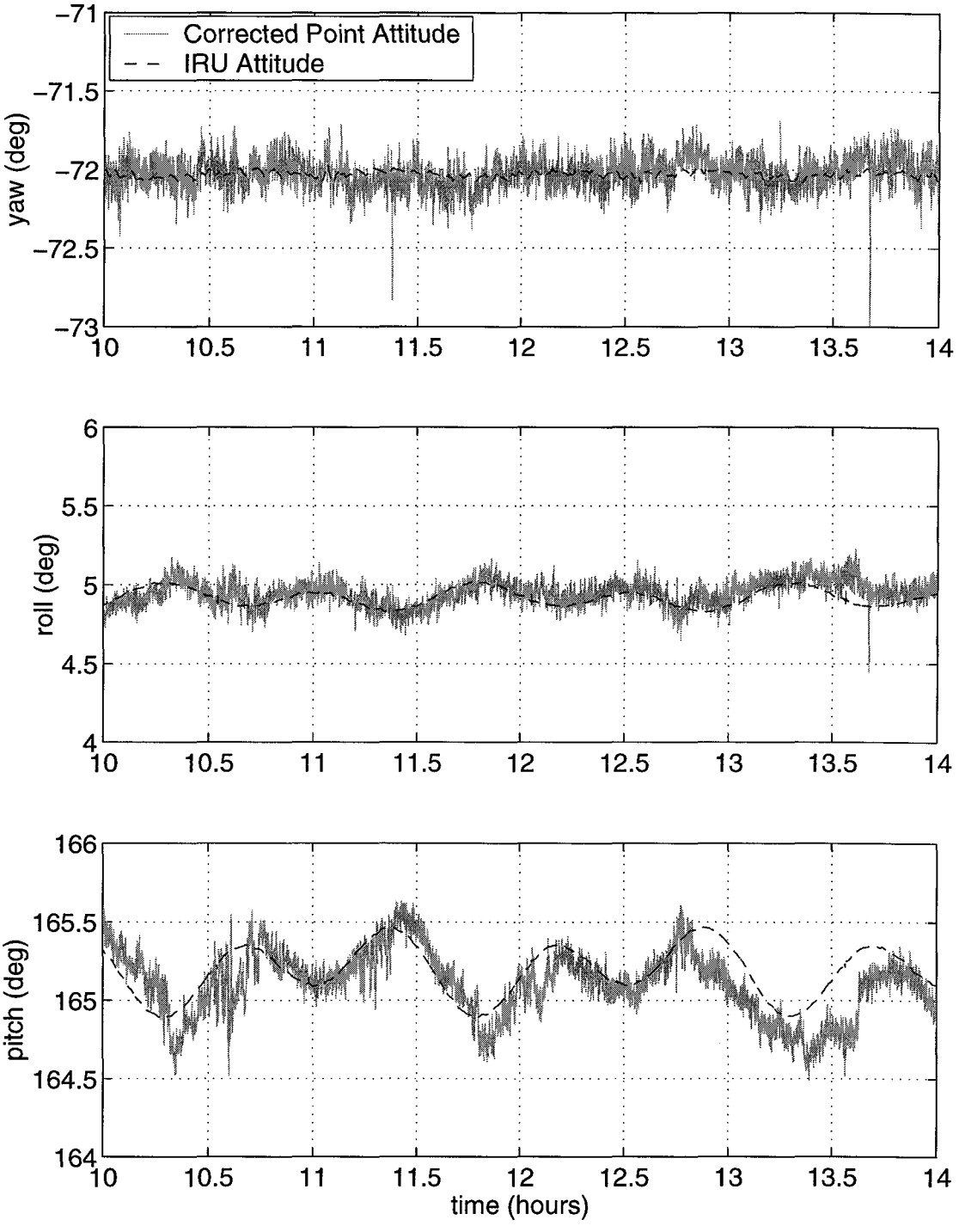
Corrected Point Attitude
IRU Attitude
yaw (deg)
roll (deg)
pitch (deg)
time (hours)
−71
−71.5
−72
−72.5
−73
6
5.5
5
4.5
4
166
165.5
165
164.5
164
10
10.5
11
11.5
12
12.5
13
13.5
14

Figure 11

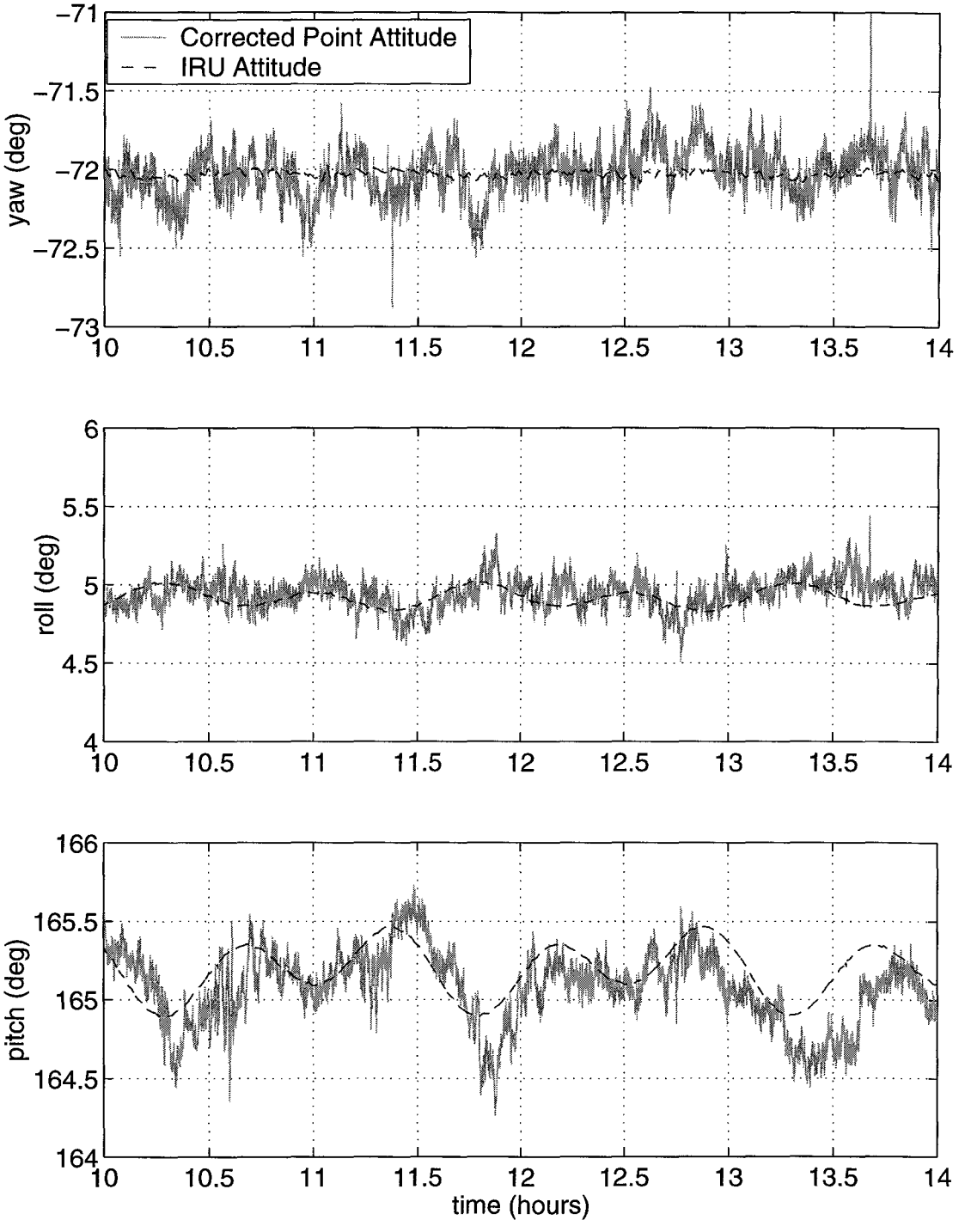
Corrected Point Attitude
IRU Attitude
yaw (deg)
roll (deg)
pitch (deg)
time (hours)
−71
−71.5
−72
−72.5
−73
6
5.5
5
4.5
4
166
165.5
165
164.5
164
10
10.5
11
11.5
12
12.5
13
13.5
14

Figure 12